

Failure Investigation for an AR Open-Graded Friction Course in Sweden

Prepared by

Jeffrey J. Stempihar, P.E.

Graduate Research Associate

Kamil E. Kaloush, Ph.D., P.E.

Associate Professor

Submitted to

Swedish Road Administration

Vägverket

405 33 Göteborg

Kruthusgatan 17, Sweden

February 2010



Ira A. Fulton Schools of Engineering

Department of Civil, Environmental and Sustainable Engineering

Tempe, Arizona 85287-5306, United States of America

Table of Contents

1.0 PROJECT STATEMENT	3
2.0 ASPHALT-RUBBER MIX	3
2.1 Asphalt Rubber Binder Characterization	3
2.1 Asphalt Rubber Mix Design	4
2.2 Asphalt Rubber Mix Test Results (SRA).....	4
2.3 Construction Conditions	5
3.0 PAVEMENT FAILURE.....	6
4.0 ASU TESTING.....	7
4.1 Asphalt-rubber Binder Testing (ASU).....	8
4.2 Initial Specimen Compaction (ASU)	10
4.3 Experimental Design.....	12
4.3 Specimen Preparation	12
4.3 Dynamic Modulus Testing.....	13
4.3 Triaxial Shear Testing.....	16
5.0 STATISTICAL ANALYSIS	19
6.0 CONCLUSION.....	20
7.0 REFERENCES	22
Appendix A.....	23
Appendix B	27
Appendix C	32

1.0 PROJECT STATEMENT

During the fall of 2008, a contractor placed an asphalt-rubber, open-graded friction course on a highway in Norrköping, Sweden as part of a construction contract. Within six weeks of placement, severe raveling caused numerous safety issues on the highway. A decision was made to remove and replace the friction course only eight weeks after placement. The Swedish Road Administration (SRA) has requested that Arizona State University (ASU) investigate possible causes of failure in the pavement. Results of this independent investigation will be compared with a parallel study being conducted by SRA.

2.0 ASPHALT-RUBBER MIX

Mix design data were provided to ASU by the Swedish Road Administration. Information included asphalt binder characterization, mix design details, asphalt performance testing and a summary of construction conditions and testing. A summary of the information provided by the SRA is included in this section.

2.1 Asphalt Rubber Binder Characterization

According to SRA, rubber mixed with the binder for this project consisted mainly of truck tires with a gradation 0-1.5 mm and the final asphalt blend consisted of 82% asphalt binder and 18% rubber. A summary of the test data for the asphalt binder is displayed in Table 2.1 whereas, actual test reports can be found in Appendix A.

Table 2.1 – SRA test data for asphalt rubber binder.

Test	Trial 1	Trial 2
ASTM D5 Needle Penetration (4° C)(1/10 mm)(EA)(E)	17	12
ASTM D5 Softening Point (°C) (EA) (E)	67.4	70
SS EN 1426 Needle Penetration (25° C) (1/10 mm)(E)	31	36
ASTM D59 Resilience % (EA) (E)	44	51
Rotational Viscosity (177° C)(Pa)(EA)(E)	2.9	4.2

SRA reported that the higher rotational viscosity value of 4.2 Pa-s was taken after the binder remained in the tank overnight. Typically this is due to settling of the rubber particles in the binder.

2.1 Asphalt Rubber Mix Design

The mix design report developed for the asphalt-rubber, open -graded rubber friction course used in the project can be found in Appendix A. Table 2.2 provides a brief summary of key mix parameters in this study.

Table 2.2 – SRA mix design parameter summary

Mix Properties	SRA Value
Binder Content (%)	8.8
G_{mm} (g/cm ³)	2.388
Marshall Air voids, (%)	19
Aggregate Crush Count (%)	100
Anti-Stripping Agent (cement) (%)	1
Minimum Air Voids (%)	15

From this table, it is important to note that this mix design has a minimum air void specification of 15% in the field.

2.2 Asphalt Rubber Mix Test Results (SRA)

SRA performed several tests on the asphalt binder and mix. Overall, the asphalt-rubber binder and mix performed sufficiently in all tests that were completed before construction. These tests included:

- SC-T-90 Binder drain down
- SS-EN 12697-11 Rolling bottle analysis
- FAS 446 Indirect tensile strength ratio (ITSR)
- SS-EN 12697-17 Cantabro test

According to SRA, there was only 0.1% drain down by mass in the mix with binder content of 8.5%. These test results indicate the mix should not be susceptible to binder drain down after construction. In the rolling bottle analysis, actual stones were selected from the mix and subjected to the test to determine the binder coverage on the aggregate after a specified time of rolling. According to this test, aggregate still had nearly 100% of coverage of binder even after approximately 75 hours of rolling. Results of the ITSR were reported to be 93%. This value is a good indicator that the mix would not be susceptible to moisture damage. In the Cantabro test, the percent loss of dry laboratory compacted Marshall specimens was 12%.

After failure of the mix, SRA subjected additional specimens to the Cantabro test. Three 60 mm slabs with approximately 15% air voids were prepared using a roller compactor. The first slab was compacted directly from the production mix. The second slab was performed from aggregate from Adelöv and asphalt-rubber from production. Finally, the third slab was compacted from aggregate from Adelöv and from laboratory mixed asphalt-rubber from the same production sources. Using cores from these slabs, two Cantabro tests were performed on specimens from each slab. The first test was performed in accordance with the test method. For the second test, the sample was conditioned according to the ITSR test and then exposed to the Cantabro test. Dry samples from the first slab had a mean percent loss of 25% whereas the conditioned samples showed a mean percent loss of 70%. At the time of this report, data were not available for the second and third slabs. The large percent loss value of the production mix samples serves as a good indicator that the mix placed in the field may have had a high susceptibility to moisture damage.

2.3 Construction Conditions

The following is a summary of climate conditions during construction and construction test results:

- Sunny with 10 -13°C air temperatures,
- Mixing temperature was approximately 165°C ($\pm 5^\circ\text{C}$),
- Mix transportation distance after production was 20-25 km,
- A heater was used to bring surface temperatures to 30 - 50°C before paving,
- Contractor used a paver system that applied tack coat immediately prior to paving.
- Latex modified emulsion was applied at a rate of 0.5 – 0.6 kg/m².
- Lifts were placed in 40-50 mm thickness
- Static rollers were used for compaction
- Pavement temperature were approximately 80°C when final compaction was achieved, and
- Air voids of the pavement cores were in the range of 15 – 17 %.

Although no climate data is available in the weeks following construction, SRA believes that temperatures were cool during the days following construction and may have been below 0°C

during some of the nights. Typically, this region of Sweden has wet and cool weather during the time of year after construction was completed.

SRA provided several pictures during the construction process. Figure 2.1 is an overall view of the mix during paving operations. A close-up photo of the mix after paving and compaction is displayed in Figure 2.2.



Figure 2.1 - Paving of asphalt-rubber OGFC in Norrköping, Sweden.



Figure 2.2 – Pavement surface immediately following paving and compaction.

3.0 PAVEMENT FAILURE

SRA reported that the asphalt-rubber mix placed on the highway began to fail approximately 4-6 weeks following construction. The first signs of failure were in the form of raveling on the pavement surface. After 8-9 weeks of service, SRA removed and replaced the pavement to avoid monetary claims for damage to windshields and cars. Figure 3.1 displays the pavement surface prior to replacement. Loss of binder from the aggregate in the wheel paths is evident in the figure. Figure 3.2 shows an example of loose stones on the pavement surface due to raveling.



Figure 3.1 – Pavement surface prior to replacement.



Figure 3.2 – Loose aggregate on the pavement surface due to raveling.

The extent of the binder loss is shown in Figure 3.3. Nearly all the asphalt binder was removed from the surface of the aggregates in the trafficked areas. Raveling is also evident in the areas of pavement that did not receive traffic as shown in Figure 3.4.



Figure 3.3 – Pavement surface in trafficked areas prior to replacement.



Figure 3.4 – Pavement surface in un-trafficked areas prior to replacement.

Figures in this section depict the severity of the raveling on the pavement constructed as part of this project. According to SRA, there are no other examples of failures with this mix nor has it been used in any other paving projects. At the current time, use of this mix has been suspended pending the results of the investigation.

4.0 ASU TESTING

Upon receiving samples of production mix used during the project, the research team at ASU began by performing independent testing on mix properties to verify data provided by SRA. Preliminary tests included verification of theoretical maximum specific gravity, asphalt penetration values, softening point data and viscosity numbers. ASTM standard methods for each test are as follows:

- Theoretical Maximum Specific Gravity (ASTM D2041-03a)
- Standard Penetration Test (ASTM D5-05a)
- Softening Point (ASTM D 36-95)
- Rotational Viscosity (ASTM D 4402-87)

The G_{mm} obtained in the ASU lab was 2.381 which is within the allowable multi-laboratory precision value of 0.016 when compared to the SRA G_{mm} value of 2.388.

4.1 Asphalt-rubber Binder Testing (ASU)

Standard binder testing was performed on the asphalt-rubber binder obtained from production during the construction project. Table 4.1 provides a summary of the binder testing performed at the ASU laboratory. All testing was performed in accordance with ASTM standards and test data can be found in Appendix B.

Table 4.1 – Summary binder testing data obtained from ASU laboratory.

ASU Test	Average Value
Standard Penetration Value (4° C)(1/10 mm)	3.5
Standard Penetration Value (13° C)(1/10 mm)	7
Standard Penetration Value (25° C)(1/10 mm)	22
Standard Penetration Value (32° C)(1/10 mm)	33
Softening Point (°C)	66.3
Brookfield Rotational Viscosity (121 °C)(Pa-s)	7.52
Brookfield Rotational Viscosity (143 °C)(Pa-s)	3.02
Brookfield Rotational Viscosity (165 °C)(Pa-s)	2.73
Brookfield Rotational Viscosity (188 °C)(Pa-s)	2.07

Data presented in Table 4.1 have some similarities with data obtained by SRA and shown in Table 2.1. The standard penetration values are similar for 25°C but vary at 4°C. In addition, the softening point of 66.3°C obtained at ASU is close to SRA value of 68.7°C. The rotational viscosity value of 2.9 Pa-s at 177°C obtained by SRA for the asphalt-rubber binder is within the range of the values obtained at the ASU laboratory.

Most asphalt binders, exhibit a linear relationship when plotted on a log-log viscosity (centipoise) versus log temperature (in degree Rankine: $R = F + 459.7 F$) scale. The approach uses only viscosity units in centipoise to define the viscosity-temperature relationship (1 Pascal second = 10^4 cP). In order to make use of all consistency tests variables over a wide range of temperatures, it is necessary to convert all penetration (pen) and softening point (TRB)

measurements into viscosity units. Penetration data is converted to viscosity units by the following model developed at the University of Maryland as a part of a Strategic Highway Research Program (SHRP) study¹.

$$\log \eta = 10.5012 - 2.2601 \times \log (\text{pen}) + 0.00389 \times \log (\text{pen})^2 \quad \text{Equation 1}$$

Equation 1 shows the relationship to obtain the viscosity from penetration results in poises. The second consistency variable point defined by the softening point (TRB) is converted to viscosity units by the approach suggested by Shell Oil researchers. It states that all asphalts at their softening point (TRB), will yield a penetration of approximately 800 and a viscosity of 13,000 poises. The third group of viscosity values at high temperature is obtained with the rotational viscosity test with the use of the Brookfield Viscometer.

Using the above three methods, all penetration and softening point results can be shown or converted to viscosity units (cp), which together with the rotational viscosity test results can then be used as direct viscosity measurements to obtain a viscosity (η) - temperature (T_R) relationship from the following regression equation:

$$\log \log \eta (\text{cp}) = A_i + VTS_i \times \log T_R \quad \text{Equation 2}$$

In Equation 2, A_i and VTS_i represents regression coefficients, which describe the unique consistency-temperature relationship of any blend. The VTS term in this equation represents the slope of the regression equation, which is also interpreted as the Viscosity Temperature Susceptibility parameter.

Figure 4.1 presents a comparison of the temperature-viscosity relationships constructed using SRA and ASU binder test data. According to the comparison, the slopes of the lines are very similar. The shift in ASU test data from SRA are typical test results for an aged asphalt binder. In this case, the binder aged from the time of production until it reached the laboratory at ASU. From the data, it can be concluded that testing at ASU confirmed initial binder test data provided by SRA.

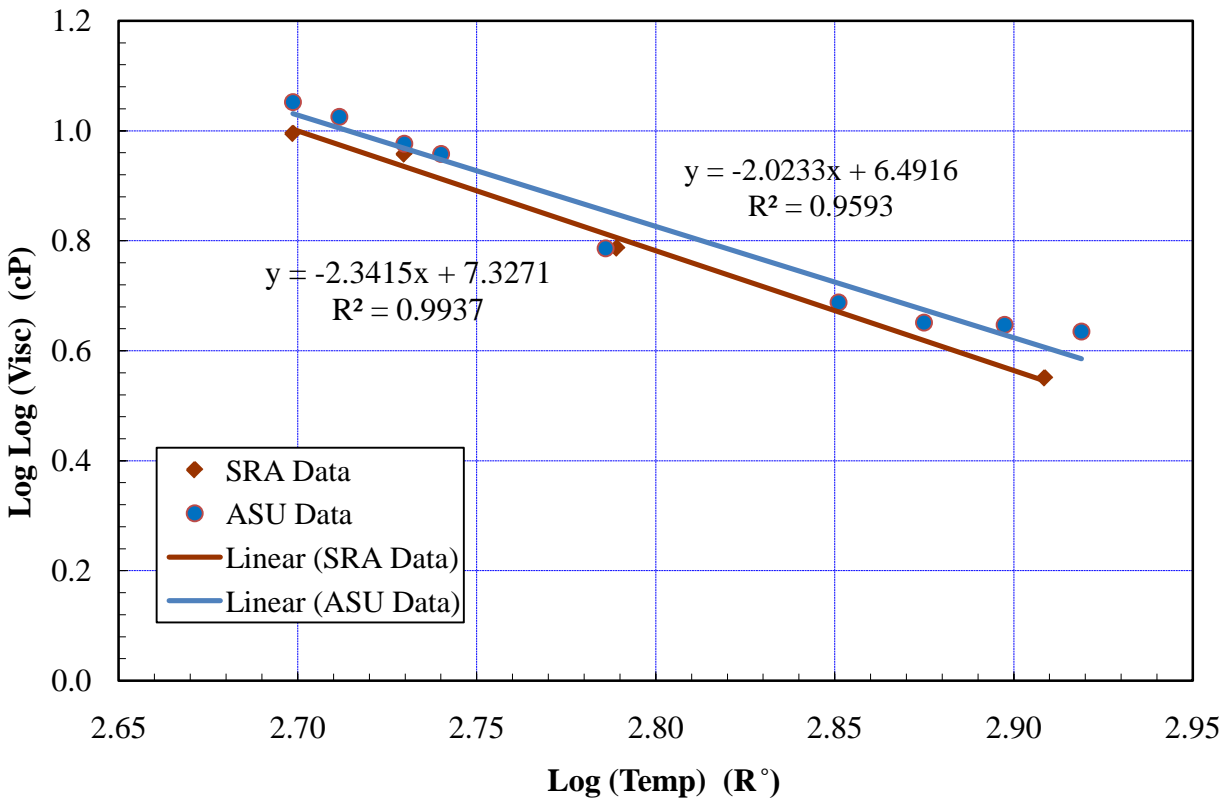


Figure 4.1 – Comparison of viscosity-temperature relationships for asphalt-rubber binder.

4.2 Initial Specimen Compaction (ASU)

Specimens were compacted using an IPC gyratory compactor. Compacted specimens were 150 mm in diameter by 170 mm tall. Using these compacted specimens, 100 mm diameter test samples were cored from the gyratory specimen and then the ends trimmed to a final height of 150 mm. Photographs of the compacted specimens can be found in Appendix B.

Initial samples compacted at approximately 17% air voids exhibited extensive aggregate fracturing, especially at the edges of the aggregate. Figure 4.2 shows an example of the aggregate fracturing of numerous aggregates in the sample.

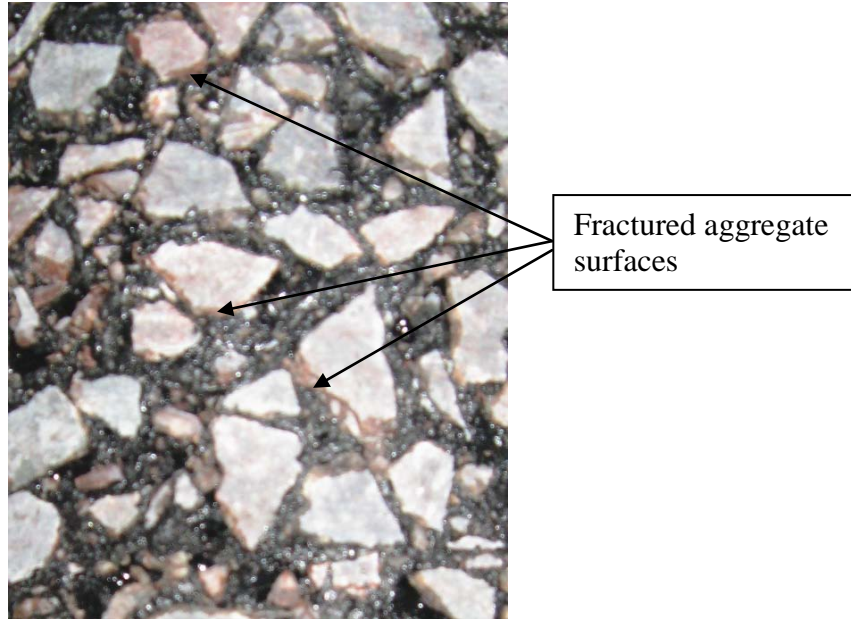


Figure 4.2 – Fractured aggregate surfaces after compaction.

Gyratory shear plots were also analyzed and for the 17% air void sample, the maximum shear strength was obtained prior to reaching the desired level of compaction. In other words, the shear stress reached a peak and began to decrease as a result of aggregate fracturing. This is graphically shown in Figure 4.3. Figure 4.4 and 4.5 present gyratory shear plots for typical 19% and 21% air void samples, respectively. In all three figures, the shear stress peaked around 500-510 kPa but reduced to around 460 kPa for the 17% air void sample. It is important to note that actual air voids of the in place pavement were between 15-17% and that if aggregate fracturing occurred at 17% air voids, it is certain that more fracturing occurred at the 15% air void level. Gyratory shear plots for all samples can be found in Appendix B.

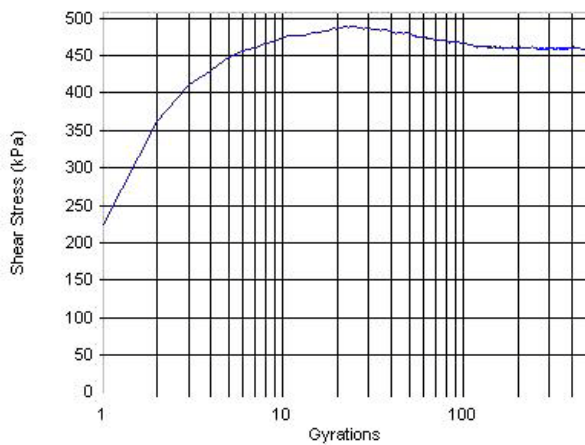


Figure 4.3 - Gyratory shear plot (17% Va)

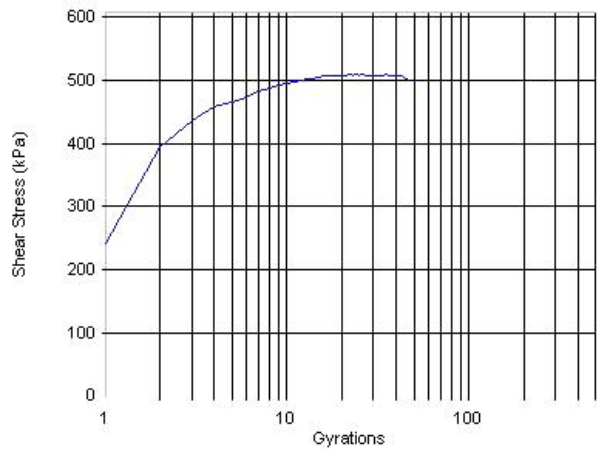


Figure 4.4 - Gyratory shear plot (19% Va)

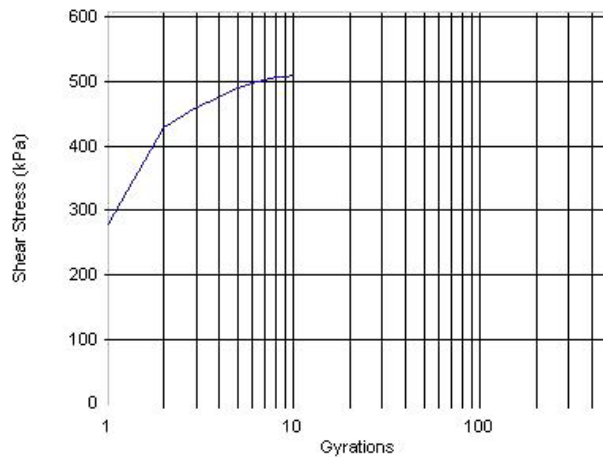


Figure 4.5 - Gyratory shear plot (21% Va)

4.3 Experimental Design

Using information collected during initial specimen compaction, it was hypothesized that failure of the asphalt-rubber OGFC may have accelerated due to weak bonds created by surface fracturing of the aggregates. The application of traffic caused the loose aggregate to be pulled from the surface resulting in the raveling shown in previous figures. Figure 3.3 may be a result of uncoated aggregate left behind after fractured pieces were removed due to raveling. Also, this failure mechanism may have been accelerated due to moisture damage and cold temperatures immediately after construction. Moisture damage may have caused the damage observed in non-trafficked areas.

In order to support the hypothesis, three specimens were compacted to each of the following air void levels to observe the fractured aggregates and gyratory shear plots:

- 17 % to represent compaction in the field
- 19 % to represent the mix design air voids
- 21 % to represent typical OGFC compaction levels in Arizona, USA.

In addition, the compacted specimens were subjected to the dynamic modulus test and triaxial shear strength tests.

4.3 Specimen Preparation

The following observations were made after preparing final specimens for testing:

1. The most fractured aggregate surfaces were observed in specimens with the lowest air void percent.
2. During compaction of the 17% air void specimens, the gyratory compactor reached a user defined maximum gyrations of 500 before the desired 170 mm height was achieved.
3. Gyratory shear plots of 17% air void specimens reached a max shear stress prior to completion of compaction indicating fracture of aggregates and additional densification.
4. Higher air void specimens only exhibited minimal surface fracturing

Photographs of the compacted specimens and gyratory shear plots can be found in Appendix B. Observations after compaction support the initial finding that aggregate fracturing occurred during laboratory compaction.

Using the Corelok method, air voids were determined for all laboratory compacted samples. A summary of the sample air voids is presented in Table 4.2. Measured air voids were very close to the target values of 17, 19 and 21%.

Table 4.2 – Specimen air voids (Corelok).

Sample	Target Air Voids, %	CoreLok Air Voids, %
FSMU17 - Rep 1	17	16.9
FSMU17 - Rep 2	17	16.6
FSMU17 - Rep 3	17	16.7
FSMU19 - Rep 1	19	19.2
FSMU19 - Rep 2	19	18.7
FSMU19 - Rep 3	19	19.3
FSMU21 - Rep 1	21	21.2
FSMU21 - Rep 2	21	20.4
FSMU21 - Rep 3	21	21.2

4.3 Dynamic Modulus Testing

The stiffness response of hot mix asphalt (HMA) materials under repeated traffic loading is a very important parameter used in current pavement design methods². The dynamic complex modulus test is used to capture the response of HMA under continuous loading. The dynamic complex modulus can be defined by the following equation²:

$$E^* = \frac{\sigma}{\epsilon} = \frac{\sigma_o * \sin(\omega t)}{\epsilon_o * \sin(\omega t - \varphi)}$$

Equation 3

where:

- σ_o = peak (maximum) stress
- ϵ_o = peak (maximum) strain
- φ = phase angle, degrees
- ω = angular velocity

The dynamic modulus is simply the absolute value of the complex modulus and can be expressed using the following equation²:

$$|E^*| = \frac{\sigma_o}{\epsilon_o}$$

Three samples from each air void group were subjected to an unconfined dynamic modulus test at 70°F to evaluate the mix stiffness properties. Applied load frequencies were 25, 10, 5, 1, 0.5 and 0.1 Hz. Figure 4.3 graphically displays a comparison of dynamic modulus values while tabular data can be found in Table 4.6.

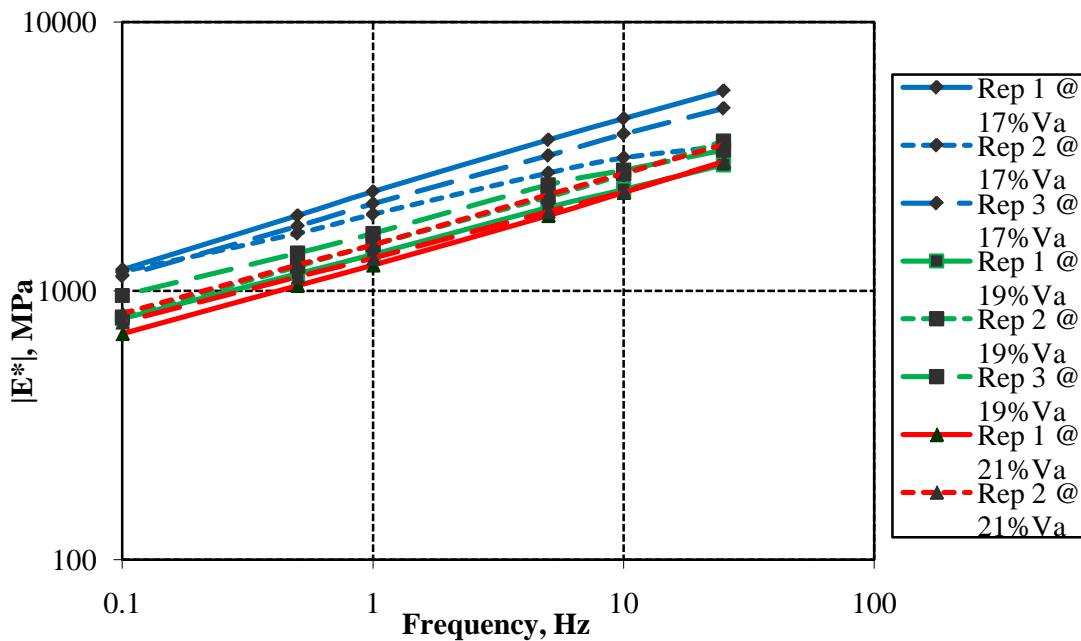


Figure 4.6 – Dynamic modulus versus loading frequency for Swedish OGFC.

Table 4.3 – Dynamic modulus test data for Swedish OGFC.

Mix I.D.	Mixture Description	Temp. °F	Freq. Hz	Dynamic Modulus, E* (MPa)						Phase Angle, ϕ (degree)					
				Rep1	Rep2	Rep3	Avg. E*	St. Dev.	%CV	Rep1	Rep2	Rep3	Avg. ϕ	St. Dev.	%CV
FSMU17	Swedish OGFC Unconfined 17% Va	70	25	5549	3459	4779	4504	1057	23	21	27	23	23.5	3.1	13
			10	4376	3130	3836	3753	625	17	23	25	23	23.3	1.1	5
			5	3647	2749	3191	3198	449	14	24	25	25	24.7	0.3	1
			1	2342	1930	2112	2128	206	10	29	28	28	28.5	0.2	1
			0.5	1907	1638	1741	1762	136	8	31	30	29	29.8	0.8	3
			0.1	1199	1180	1135	1171	33	3	34	35	31	33.0	2.0	6
FSMU19	Swedish OGFC Unconfined 19% Va	70	25	2947	3615	3345	3146	336	11	25	29	27	26.9	1.9	7
			10	2385	2720	2814	2600	226	9	24	29	28	26.8	2.6	10
			5	2045	2237	2482	2264	219	10	26	29	26	26.9	1.8	7
			1	1368	1487	1636	1502	134	9	30	32	30	30.6	1.2	4
			0.5	1159	1234	1382	1271	113	9	32	33	31	32.0	1.2	4
			0.1	789	800	962	876	97	11	35	35	32	34.0	1.3	4
FSMU21	Swedish OGFC Unconfined 21% Va	70	25	3017	3501	3032	3025	275	9	25	21	28	24.8	3.6	14
			10	2328	2736	2340	2334	232	10	26	26	26	25.7	0.1	0
			5	1910	2280	1975	1943	198	10	26	28	27	26.9	0.6	2
			1	1249	1483	1325	1287	119	9	31	30	31	30.7	0.9	3
			0.5	1048	1249	1128	1088	101	9	32	32	33	32.4	0.6	2
			0.1	694	823	767	731	65	9	36	34	37	35.5	1.3	4

According to Figure 4.3, the samples with 17% air voids had the highest dynamic modulus values across all loading frequencies. Samples with 19% and 21% air voids appear to have similar dynamic modulus values. Table 4.3 presents the mean, standard deviation and coefficient of variation (CV) values for three replicates of a mix at each frequency. CV values indicate some variability in the data especially for higher loading frequencies. The highest variability was in the 17% air void samples at 25, 10 and 5 Hz.

4.3 Triaxial Shear Testing

The triaxial shear strength test has been used for many years in attempt to characterize an asphalt mixes susceptibility to permanent deformation. However, due to the difficulty of performing the test and specialized test equipment, this test has not been used as frequently as repeated load tests to investigate permanent deformation.

The test is performed according to AASHTO T167 at three confining pressures to develop the Mohr-Coulomb failure envelope. The mathematical model for this failure envelope is as follows²:

$$\tau = c + \sigma * \tan \phi \quad \text{Equation 4}$$

where:

τ = shear stress,

c = intercept or cohesion parameter,

σ = normal stress and

ϕ = slope of failure envelope or angle of internal friction.

According to Equation 4, the shear strength of an asphalt mixture depends on the cohesion parameter (c), normal stress (σ) and the angle of internal friction (ϕ). The cohesion parameter represents the bonding effect of the asphalt binder in the mixtures whereas the angle of internal friction describes the ability of the aggregate structure to resist shear stress when an axial load is applied. According to NCHRP Report 465, the c and ϕ parameters can vary significantly with applied load rate, temperature and HMA volumetrics².

The triaxial shear strength test was performed on mixes using samples 150 mm in height and 100 mm in diameter³. Testing was performed at 37.8°C with confining pressures of 0, 138 and 276 kPa. The specimens were loaded with a constant strain rate of 1.27mm/mm/min until failure.

The results of the triaxial strength test can be found in Table 4.4. It is important to note that test data were not obtained for the 21% air void samples at 276 kPa confinement pressure. During the test, large gaps in the sample aggregate structure punctured the membrane necessary to achieve confinement.

Table 4.4 – Triaxial test results summary.

Air Voids (%)	σ_3 (kPa)	Maximum σ_1 (kPa)	Strain @ Failure	Time @ Failure (Sec)
17	0	340	2.1	210
	138	920	6.8	500
	276	1250	3.8	280
19	0	245	2.6	190
	138	860	11.9	870
	276	820	9.2	680
21	0	180	2.7	200
	138	820	17.4	1280
	276	n/a	n/a	n/a

According to the results, the 17% air void samples exhibited the highest strength at shear failure followed by the 19% and 21% air void samples. Mohr-Coulomb failure envelope plots were developed using the data from Table 4.4. These plots along with data calculations can be found in Appendix C.

Using the linear regression equations from the failure envelope plots, the c and ϕ parameters were obtained. The c -parameter is simply the y -intercept of the linear equation and the ϕ parameter is the angle of the line or the inverse tangent of the slope of the line. The c and ϕ parameters are shown in Table 4.5 below. According to these data, the 17% and 19% air void samples exhibited similar c and ϕ parameters. However, the 21% air void mix data did not correspond well with the other samples given the same aggregate gradation and binder type.

Table 4.5 – C and ϕ parameters.

Mix	C	ϕ
17% Va	90.29	38.55
19% Va	85.57	32.32
21% Va	37.90	44.32

The test results of the 21% air void samples may have been limited by the fact that test data was not obtained at a confinement level of 276 kPa. Also, it is important to note that replicate samples were not tested.

Mohr-Coulomb failure envelopes for the three mixes were plotted in Figure 4.7 using Equation 2 and the values from Table 4.5. Again it is evident that the c-parameter of the 21% air void mix is much lower than the 17% and 19% mixes.

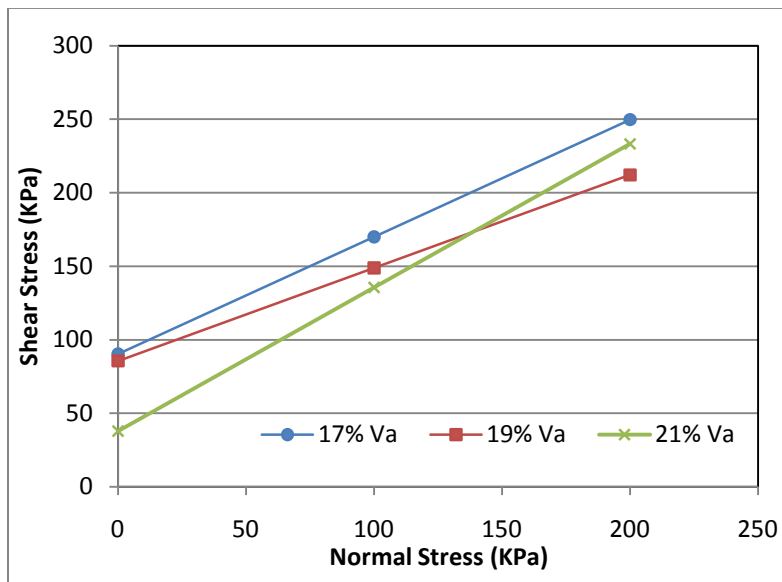


Figure 4.7 – Mohr-Coulomb failure envelope comparison.

Comparisons of the ϕ parameters indicate that the 17% air void samples had a slightly higher angle of internal friction than the 19% samples. One reason for this may have included a change in gradation due to excess aggregate crushing during compaction. The additional fractured aggregate may have lead to increased shear resistance with an applied load. Due to the limitations of the 21% air void data, these samples were not considered when making this comparison.

5.0 STATISTICAL ANALYSIS

Analysis of variance was performed on the dynamic modulus data using a 95% confidence level. Analysis of these data indicates that there are no statistical differences between dynamic modulus values for the 19% and 21% air voids samples across all loading frequencies. However, when comparing 17% to 19% and 17% to 21% air void samples, the dynamic modulus values are statistically different. This is the case for all frequencies except 25 Hz. The large variance of data at 25 Hz may have resulted in accepting the null hypothesis that data sets were indifferent. Table 5.1 presents the F-values used for statistical comparisons.

Table 5.1 – E* statistical comparison.

Frequency (Hz)	Air Void (%) Comparison	F-value	F-critical
25	17-19	4.079	7.709
	17-21	5.016	7.709
	19-21	0.225	7.709
10	<i>17-19</i>	<i>8.851</i>	<i>7.709</i>
	<i>17-21</i>	<i>11.634</i>	<i>7.709</i>
	19-21	0.844	7.709
5	<i>17-19</i>	<i>10.643</i>	<i>7.709</i>
	<i>17-21</i>	<i>16.221</i>	<i>7.709</i>
	19-21	1.375	7.709
1	<i>17-19</i>	<i>19.692</i>	<i>7.709</i>
	<i>17-21</i>	<i>31.735</i>	<i>7.709</i>
	19-21	1.945	7.709
0.5	<i>17-19</i>	<i>24.316</i>	<i>7.709</i>
	<i>17-21</i>	<i>40.279</i>	<i>7.709</i>
	19-21	1.766	7.709
0.1	<i>17-19</i>	<i>29.545</i>	<i>7.709</i>
	<i>17-21</i>	<i>95.790</i>	<i>7.709</i>
	19-21	1.752	7.709

Due to data limitations discussed in the triaxial shear strength section of this report and the lack of test replicates, statistical analysis of the data was not performed. If further replicates are tested, analyses of the data should be performed to determine statistical differences in the data.

6.0 CONCLUSION

As requested by SRA, an independent evaluation of a failed AR open-graded friction course was completed at ASU. The analysis of the binder and G_{mm} confirmed the data provided by SRA and review of the mix design and performance testing did not provide insight into a cause of failure.

After reviewing construction information, it was hypothesized that the mix was over-compacted in the field and that crushed aggregate contributed to the rapid failure of the pavement. This hypothesis was tested by compacting specimens at 17% and 19% air voids to represent field and mix design values, respectively. Additional specimens were compacted at 21% air voids for comparison as this resembles a typical value used for AR open-graded friction courses in Arizona, USA.

Gyratory shear plots confirmed the hypothesis by showing a reduction of shear stress during compaction for the 17% air void samples. Typically, this trend indicates aggregate fracturing during the compaction process. Once the samples were completed, fracturing was noticed on the surfaces of the aggregates. It is important to note that even though the 19% and 21% samples did not exhibit shear stress decline, fractured aggregates were evident after compaction. These fractured aggregates left surfaces uncoated with binder after compaction which could have been easily raveled from the surface with the application of traffic loading.

Dynamic modulus testing was performed for comparison between the samples. The test indicated that dynamic modulus values of the 17% air voids samples were greater and statistically significant ($\alpha=0.05$) in comparison to the 19% or 21% samples. There were no statistical differences between the dynamic modulus values of the 19% and 21% air void samples. These results indicate that the dynamic modulus test may not have been the best test selection to assess aggregate damage. It may be the case that the crushed aggregate in the 17% air void sample modified the gradation which resulted in higher dynamic modulus values.

Triaxial shear strength tests were also performed on the samples to compare the strength of the material. Data indicated that the 17% air void samples had the highest shear resistance when compared to the 19% samples. Due to limited test data, the 21% samples were not included in

the analysis. Comparisons of the ϕ parameters indicate that the 17% air void samples had a slightly higher angle of internal friction than the 19% samples. One possibility was that the gradation was changed due to excess aggregate crushing during compaction. The additional fractured aggregate may have lead to increased shear resistance when a load was applied.

In conclusion, field compaction to air void levels below the mix design value of 19% may have resulted in the premature failure of the AR open-graded friction course. The gyratory shear plots along with the visual inspection of the compacted samples provided evidence of excessive aggregate fracturing. Since the fractured aggregates weren't coated with binder, they may have been easily raveled from the surface. Also, this failure mechanism may have been accelerated due to moisture damage and cold temperatures experienced immediately after construction.

It is important to note that ASU testing was performed solely on laboratory compacted samples from field production mix provided by SRA.

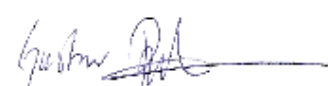
7.0 REFERENCES

¹Witczak, M.W. and Kaloush, K.E., “Performance Evaluation of CitgoFlex Asphalt Modified Mixture using Advanced Material Characterization Tests”. Department of Civil Engineering, University of Maryland, College Park, Maryland, 1998.

²NCHRP Report 465. Simple Performance Test for Superpave Mix Design. Transportation Research Board, 2002.

Appendix A


Provnnummer 81977

ANALYS Gummibitumen		Sidan 1 av 1		
Beställare Vägverket Samhälle & Trafik Lars Preinfalk Projekt gummiastfalt	Provtagningsdatum 2008-10-06 Ankomstdatum 2008-10-06	Analys start 2008-11-28 Analys slut 2008-11-28		
Produkt Gummibitumen Leverantör	Referens Provtagningsplats Skanska Ludden Provtagare	Idnummer		
Entreprenör	Märkning 6/10 kl. 13.10 visk 2,9 Pas			
Objekt				
Provresultat Kommentar	Medel- värde	Mätosäker- het +/-	Receipt	
ASTM D 5 Needle penetration (4 °C) (1/10 mm)[EA][E]	17			
ASTM D36 Softening point (°C)[EA][E]	67,4			
SS-EN 1426 Needle penetration (25 °C) (1/10 mm)[E]	31			
ASTM D5329 Resilience (%)[EA][E]	44			
Rotational Viscosity (Pas)[EA][E]	2,9			
Notering	Ort och datum Jönköping 2008-12-01			
	 Gustav Petersson, Platschef Underskriften är en elektronisk signatur			
<small> Provresultat avser endast det laboratorium som inkommit prov. För information om mätosäkerhet kontakta laboratoriet. (E) = Enkelprov (EA) = E) ackrediterad metod </small>				

Slut / Astalt - rapport utan kurva

Vägverket Produktion Beläggning	Beställadress	Telefon nr	Org. nr	E-post adress
Väglaboratoriet		038 - 31 21 30		
Herkuleevägen 62	Styrelsens säte	Telefax nr	VAT nr	Internetadress
663 02 Jönköping		038 - 31 21 38		

Figure A.1 – SRA Binder Test Report 1

ANALYS Gummibitumen		Sidan 1 av 1		
Beställare Vägverket Samhälle & Trafik Lars Preinfalk Projekt gummiastait	Provtagningsdatum 2008-10-07 Ankomstdatum 2008-10-30	Analys start 2008-11-28 Analys slut 2008-11-28		
Produkt Gummibitumen Leverantör	Referens	Idnummer		
Entreprenör	Provtagningsplats Skanska Ludden Provtagare			
Objekt	Märkning 7/10 kl. 10.30 visk 2,8 Pas			
Provresultat	Medel- värde	Mätosäker- het +/-	Receipt	
Kommentar				
ASTM D 5 Needle penetration (4 °C) (1/10 mm)[EA][E]	12			
ASTM D36 Softening point (°C)[EA][E]	70,0			
SS-EN 1426 Needle penetration (25 °C) (1/10 mm)[E]	36			
ASTM D5329 Resilience (%)[EA][E]	51			
Rotational Viscosity (Pas)[EA][E]	4,2			
Notering		Ort och datum Jönköping 2008-12-01		
		 Gustav Petersson, Platschef Underskriften är en elektronisk signatur		
<small>Provresultat avser endast BIL-laboratoriet i Jönköping prov. För information om mätosäkerhet kontakta laboratoriet. [E] = Enkelprov [EA] = Ej ackrediterad metod</small>				

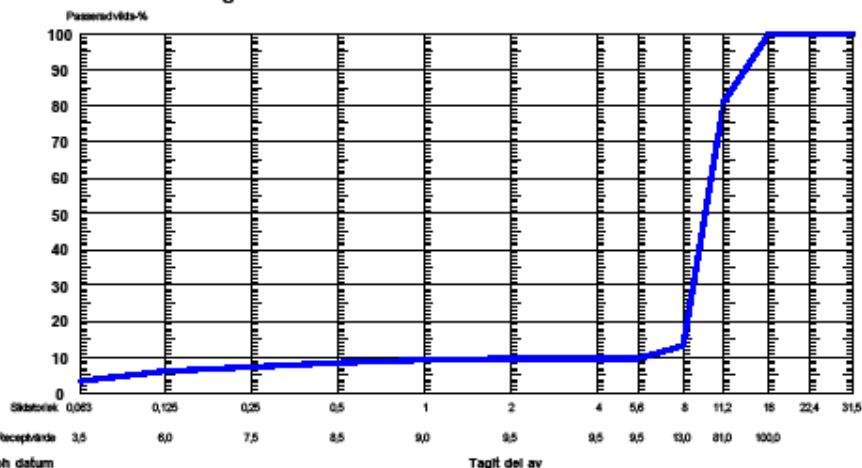
Sten / Astait - rapport utan kurva

Vägverket Produktion Beläggning	Besöksadress	Telefon nr	Org. nr	E-post adress
Väglaboratoriet		036 - 31 21 30		
Herkulesvägen 62	Styrelsens säte	Telefax nr	VAT nr	Internetadress
668 02 Jönköping		036 - 31 21 38		

Figure A.2 – SRA Binder Test Report 2

ARBETSRECEPT Beläggningssmassa		Beställare	
Produkt OGAR 11 GMB 70/100-18		Vägverket Region Sydöst	
Leverantör Skanska Ludden		Entreprenör	
Objekt Projekt Gummiasfalt		Fr.o.m datum 2008-09-11	T.o.m datum
Stenmaterial	Komdensitet (g/cm ³) 2,70	Kompaktensitet (g/cm ³) 2,388	Marshalhårum (vol-%) 18,0
Speciellt stenmaterial	Täkt Adeltöv	BFH (Bitumen Fyllt Hårum) (%) 87,0	
Leverantör	Produkt 8-11	Tillsatsmaterial	Cement 1 %
→ mm	8		
- halt vikt-%	87		
Komdensitet (g/cm ³)	2,88		
Filsighetsindex (FI)	12		
Krossytegrad (C)	100/0		
Kultivarsvärde (AN)	<5 (8 - 11,2 mm)		
Los Angelesvärde (LA)	18 (10 - 14 mm)		
Beläggningssmassa / Beläggning	Bindemedelshalt (vikt-%) 8,8	Notering	
Skrymsensitet (g/cm ³) 1,818		Bindemedelshalt = Blandning bitumen + gummi 82/18	
		Gummi: RTW0-1,5 mm	
		Hårum på färdig beläggning > 15 %	
Kontrollpunkt	0,083 2 4 8		
Passerad vikts-%	3,5 9,5 9,5 13,0		

Kornstorleksfördelning



Ort och datum
Jönköping 2008-09-29

Gustav Petersson

Gustav Petersson, Platschef
 Underskriften är en elektronisk signatur

Arbetsrecept

Vägverket Produktion Beläggning	Bestöcksadress	Telefon nr	Org. nr	Email adress
Väglaboratoriet		038 - 31 21 30		
Herkuleevägen 62	Styrelsens säte	Telefax nr	SE nr	Internetadress
663 02 Jönköping		038 - 31 21 38		

Figure A.3 – AR open-graded friction course mix design.

Appendix B



Figure B.1 – 17% Air void sample.



Figure B.2 – 19% Air void sample.



Figure B.3 – 21% Air void sample

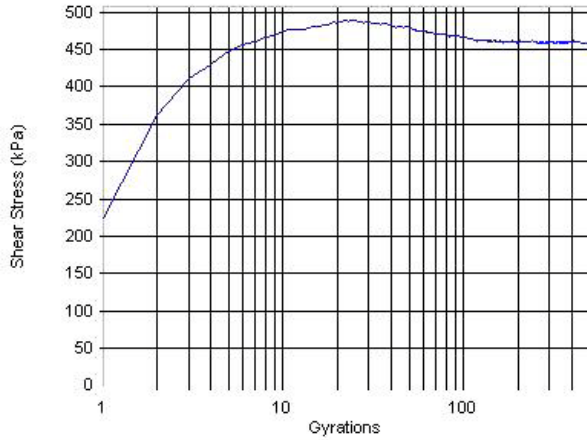


Figure B.4- Gyrotory shear plot, 17% Va – Rep 1.

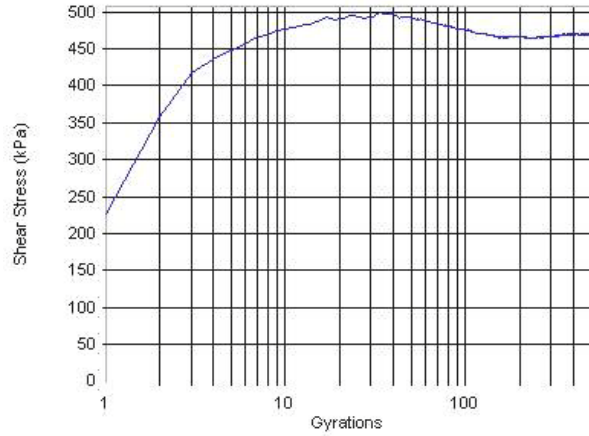


Figure B.5- Gyrotory shear plot, 17% Va – Rep 2.

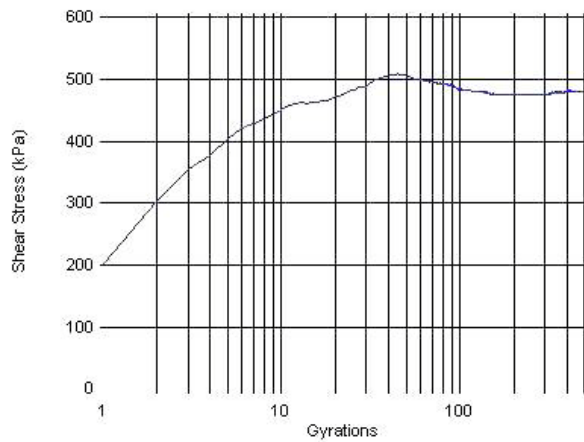


Figure B.6- Gyrotory shear plot, 17% Va – Rep 3.

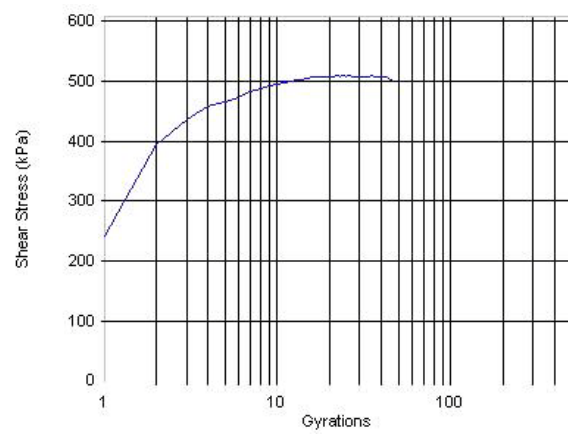


Figure B.7- Gyrotory shear plot, 19% Va – Rep 1.

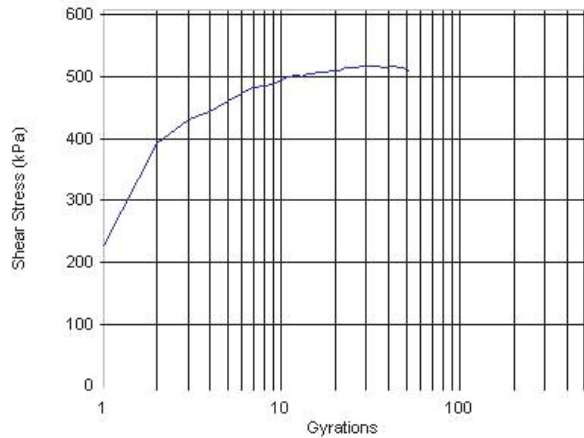


Figure B.8- Gyrotory shear plot, 19% Va – Rep 2.

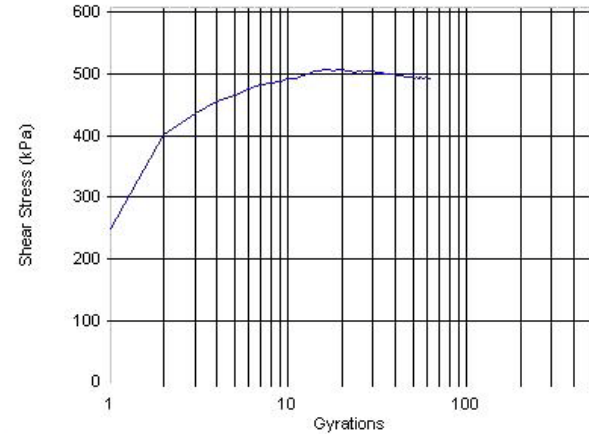
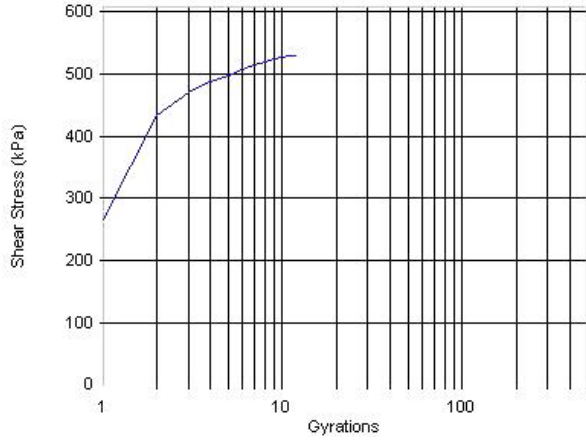
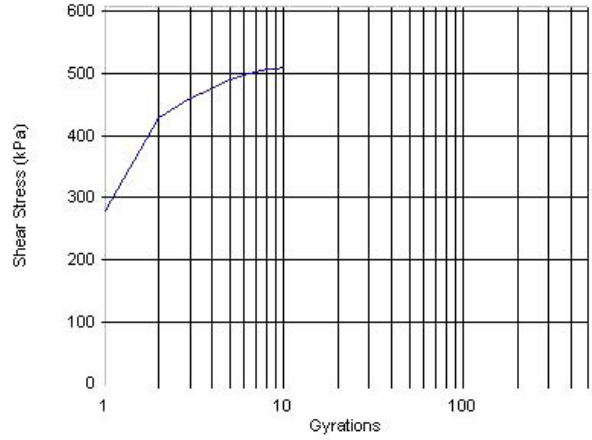


Figure B.9- Gyrotory shear plot, 19% Va – Rep 3.



**Figure B.10- Gyratory shear plot, 21% Va –
Rep 1.**



**Figure B.11- Gyratory shear plot, 21% Va –
Rep 2.**

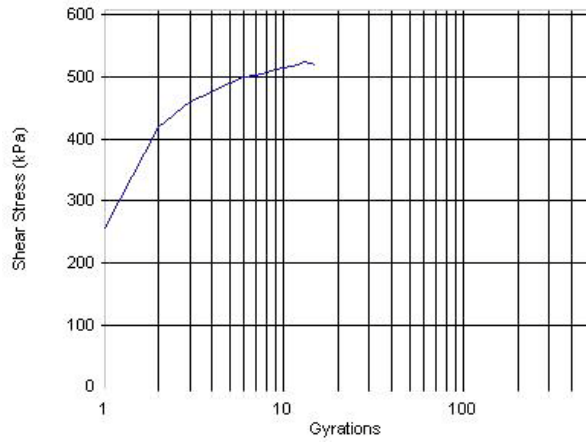


**Figure B.12- Gyratory shear plot, 21% Va –
Rep 3.**

Appendix C

Table C1 – Triaxial test data for 17% air void samples.

σ_3 (Kpa)	Sample #	Maximum σ_1 (KPa)	Strain @ Failure	Time @ Failure (Sec)
0	1	340	2.1	210
138	1	920	6.8	500
276	1	1250	3.8	280

σ_3 (KPa)	Maximum σ_1 (KPa)			Radius	Center Point	σ_1 (KPa)
	Sample 1	Sample 2	Average			
0	340.0	-	340.0	170.0	170.0	340.00
138	920.0	-	920.0	460.0	598.0	1058.00
276	1250.0	-	1250.0	625.0	901.0	1526.00

Test points	C	ϕ
0-138	74.5	42.7
0-276	82.0	38.5
138-276	160.2	33.0

σ_3 (KPa)	Normal Stress (KPa)		Shear Stress τ (KPa)	
	Tangent Points	Average	Tangent Points	Average
0	54.8	65.5	125.0	133.6
	64.2		133.1	
	77.4		142.6	
138	286.3	315.2	338.3	361.4
	311.7		360.0	
	347.5		385.8	
276	477.5	516.7	459.7	491.0
	512.0		489.2	
	560.7		524.2	

C =	90.29
ϕ =	38.55

Table C2 – Triaxial test data for 19% air void samples.

σ_3 (KPa)	Sample #	Maximum σ_1 (KPa)	Strain @ Failure	Time @ Failure (Sec)
0	1	245	2.6	190
138	1	860	11.9	870
276	1	820	9.2	680

□

σ_3 (KPa)	Maximum σ_1 (KPa)			Radius	Center Point	σ_1 (KPa)
	Sample 1	Sample 2	Average			
0	245.0	-	245.0	122.5	122.5	245.00
138	860.0	-	860.0	430.0	568.0	998.00
276	820.0	-	820.0	410.0	686.0	1096.00

Test points	C	ϕ
0-138	52.4	43.6
0-276	69.8	30.7
138-276	534.0	-9.8

Note: Negative ϕ angle removed from analysis.

σ_3 (KPa)	Normal Stress (KPa)		Shear Stress τ (KPa)	
	Tangent Points	Average	Tangent Points	Average
0	37.9	49.0	88.6	97.0
	60.0		105.4	
	-		-	
138	271.2	309.9	311.1	340.5
	348.6		369.8	
	-		-	
276	403.0	439.9	296.7	324.6
	476.8		352.6	
	-		-	

C =	85.57
ϕ =	32.32

Table C3 – Triaxial test data for 21% air void samples.

σ_3 (Kpa)	Sample #	Maximum σ_1 (KPa)	Strain @ Failure (%)	Time @ Failure (Sec)
0	1	180	2.7	200
138	1	820	17.4	1280

□

σ_3 (KPa)	Maximum σ_1 (KPa)			Radius	Center Point	σ_1 (KPa)
	Sample 1	Sample 2	Average			
0	180.0	-	180.0	90.0	90.0	180.00
138	820.0	-	820.0	410.0	548.0	958.00

Test points	C	ϕ
0-138	37.9	44.3

σ_3 (KPa)	Normal Stress (KPa)		Shear Stress τ (KPa)	
	Tangent Points	Average	Tangent Points	Average
0	27.1	27.1	64.4	64.4
	-			
	-			
138	261.5	261.5	293.3	293.3
	-			
	-			

C =	37.90
ϕ =	44.32

Note: No test data available at $\sigma_3 = 276$ kPa.

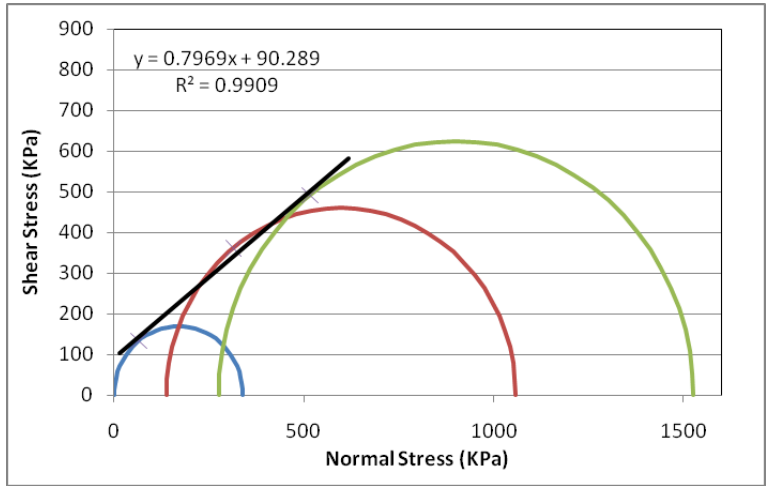


Figure C1 – Mohr-Coulomb failure envelope plot for 17% air voids.

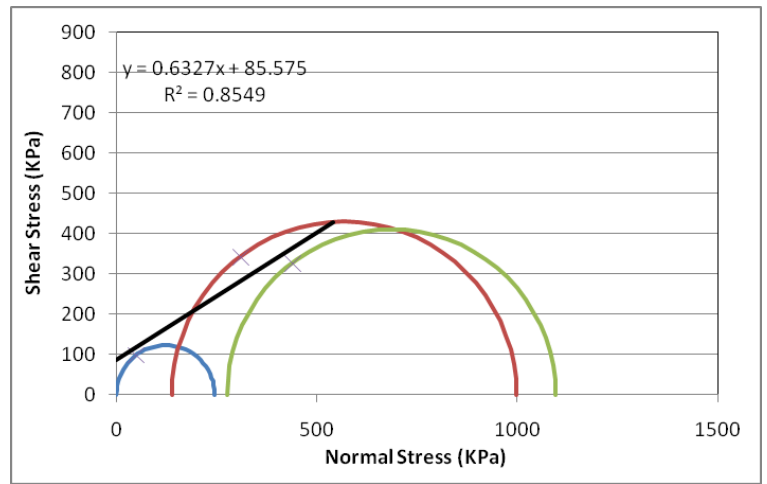


Figure C1 – Mohr-Coulomb failure envelope plot for 19% air voids.

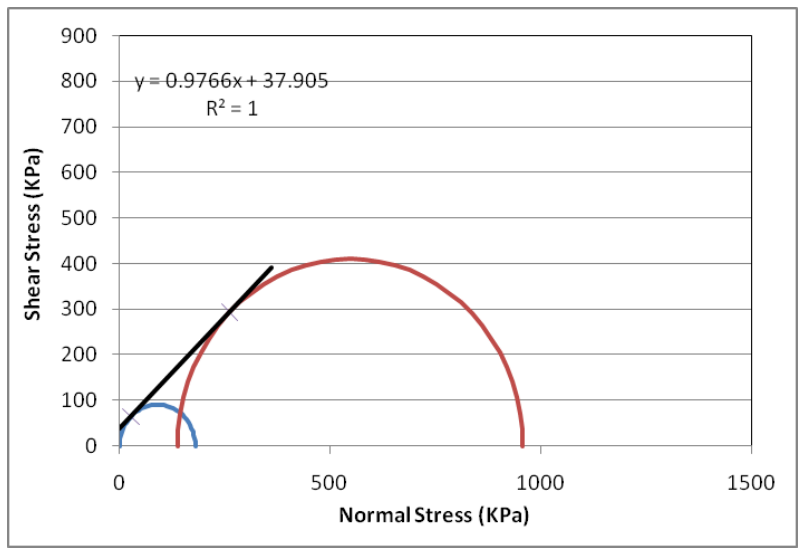


Figure C1 – Mohr-Coulomb failure envelope plot for 21% air voids.